Electronic supplementary information

Enhanced bifunctional electrocatalytic activities of hybrid $Co(OH)_2$/MOF-derived materials for green hydrogen production by electrochemical water splitting

Apurba Borah,[a] Sumit,[a] Sathishkumar Palaniyappan,[b] and Rajeshkhanna Gaddam[a]*

[a] *Department of Chemistry, National Institute of Technology Warangal, Hanumakonda-506004, India.*
[b] *Department of Physics, Centre for Functional Materials, School of Advanced Sciences, Vellore Institute of Technology, Vellore-632014, India.*

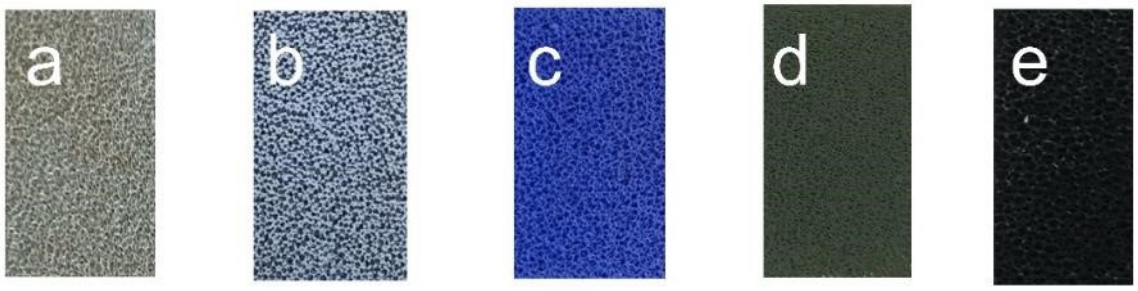

Fig. S1 Digital images of (a) bare NF, (b) $Co(OH)_2$@NF, (c) $Co(OH)_2$/ZIF-67@NF, (d) Co_3O_4@NF, (e) Co_3S_4@NF.

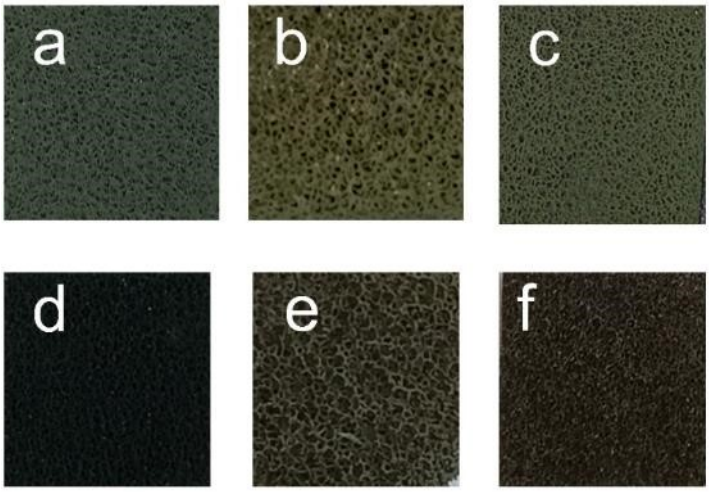

Fig. S2 Digital images of (a) Co_3O_4@NF before electrochemical studies, (b) Co_3O_4@NF after OER studies, (c) Co_3O_4@NF after HER studies @NF, (d) Co_3S_4@NF before electrochemical studies, (e) Co_3S_4@NF after OER studies, and (f) Co_3S_4@NF after HER studies, (All are of 1 cm^{-2} area).

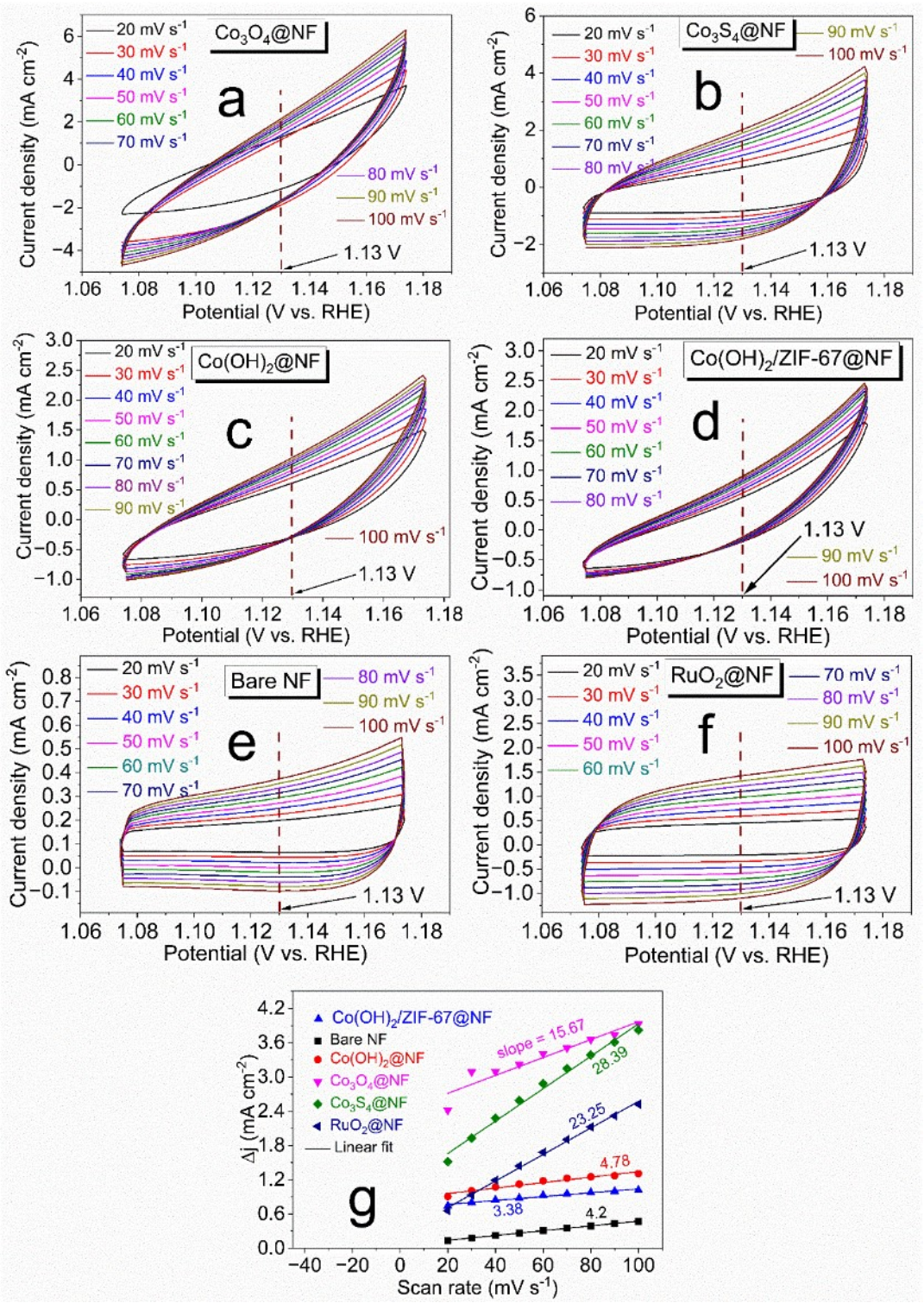

Fig. S3 Cyclic voltammograms of (a) Co_3O_4@NF, (b) Co_3S_4@NF, (c) $Co(OH)_2$@NF, (d) $Co(OH)_2$/ZIF-67@NF, (e) Bare NF, (f) RuO_2@NF at different scan rates ranging from 20 to 100 mV s^{-1}, (g) Scan rate dependent current densities of all the materials at 1.13 V (*vs.* RHE).

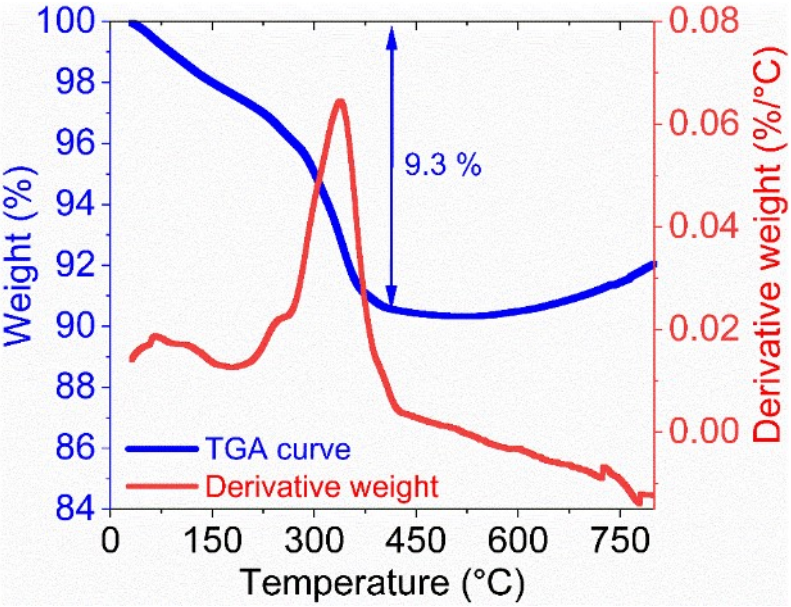

Fig. S4 TGA curve of $Co(OH)_2$/ZIF-67@NF in the presence of air.

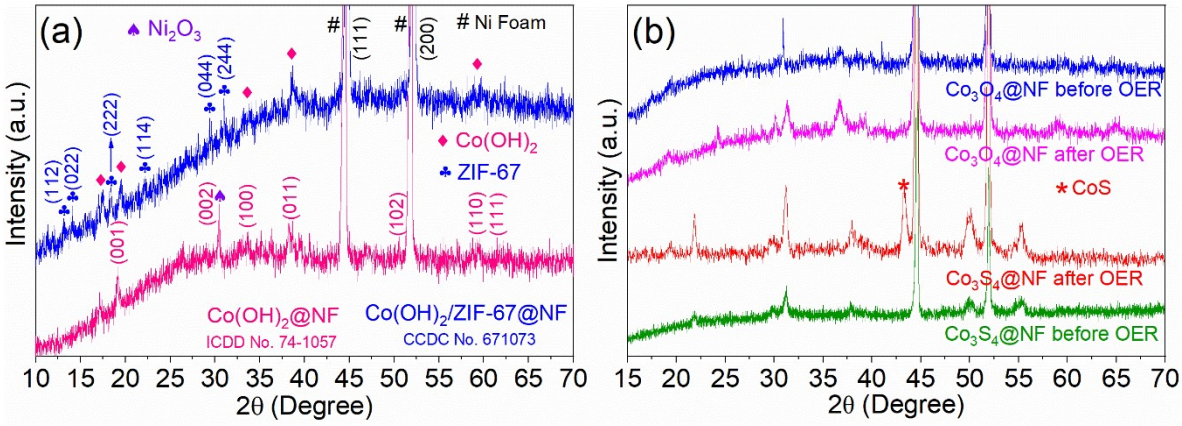

Fig. S5 PXRD patterns of (a) $Co(OH)_2$@NF, $Co(OH)_2$/ZIF-67@NF, and (b) Co_3O_4@NF and Co_3S_4@NF before and after OER studies.

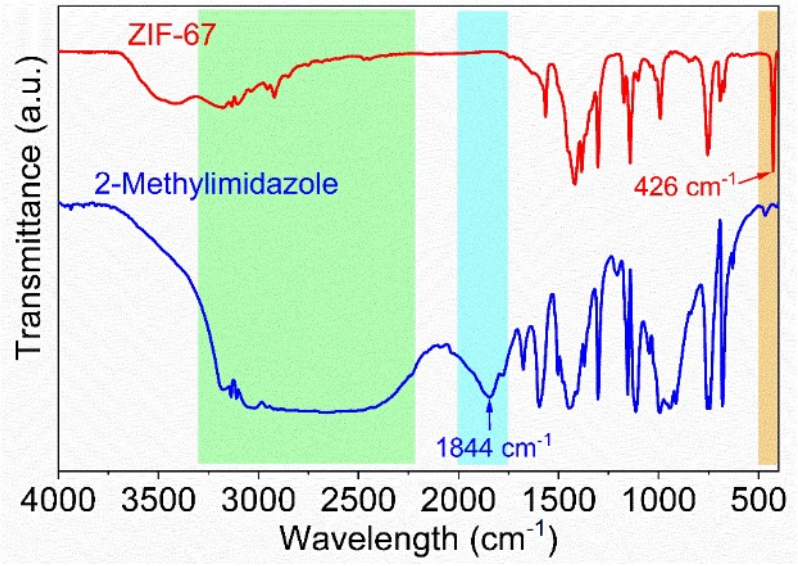

Fig. S6 FT-IR spectrum of ZIF-67 and 2-methylimidazole.

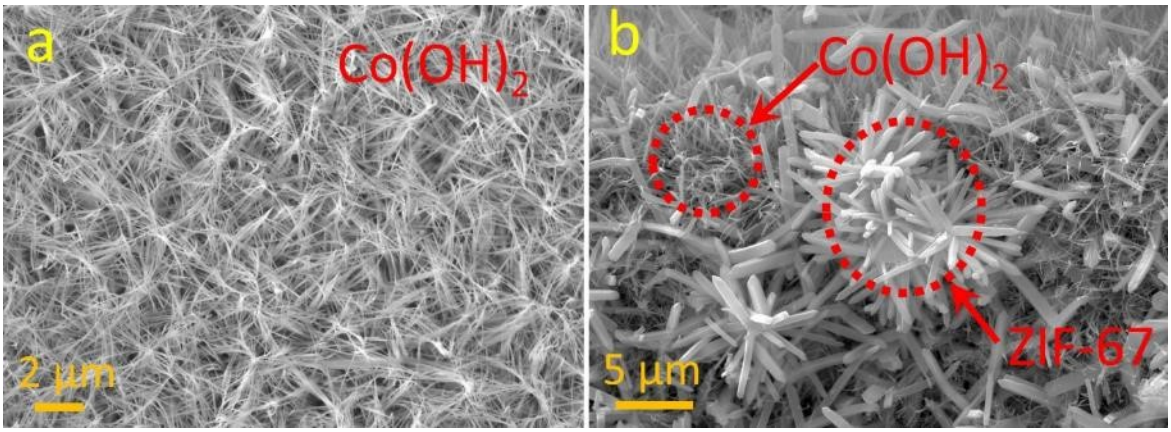

Fig. S7 The FE-SEM images of (a) $Co(OH)_2$@NF, and (b) $Co(OH)_2$/ZIF-67@NF.

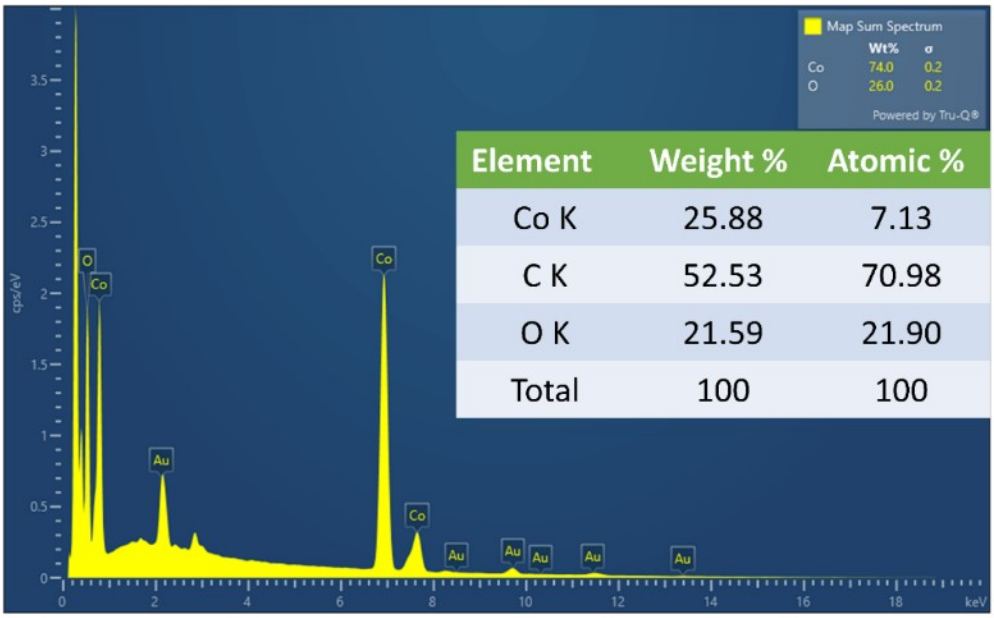

Fig. S8 EDX spectrum of Co_3O_4@NF.

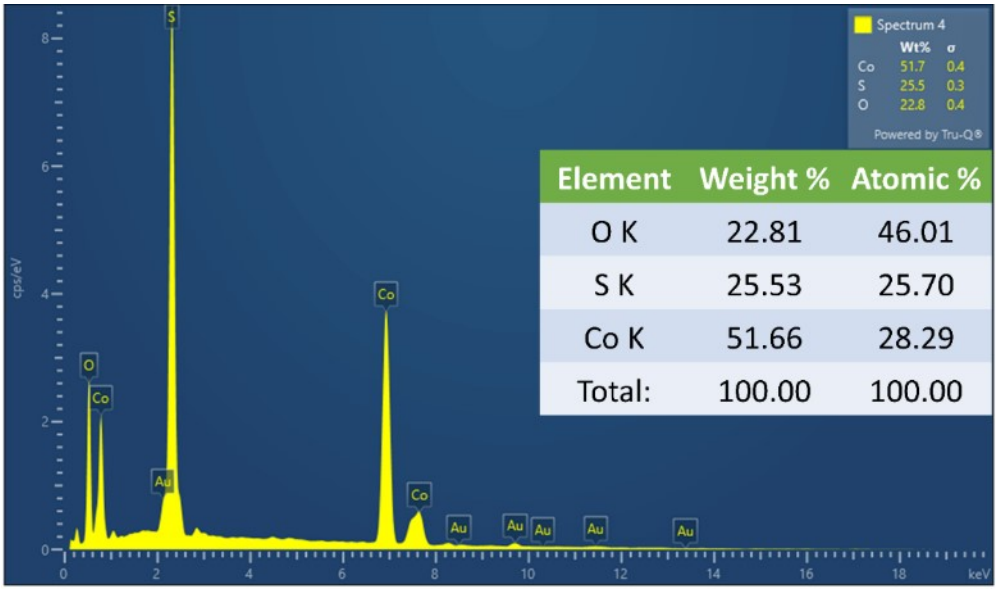

Fig. S9 EDX spectrum of Co_3S_4@NF.

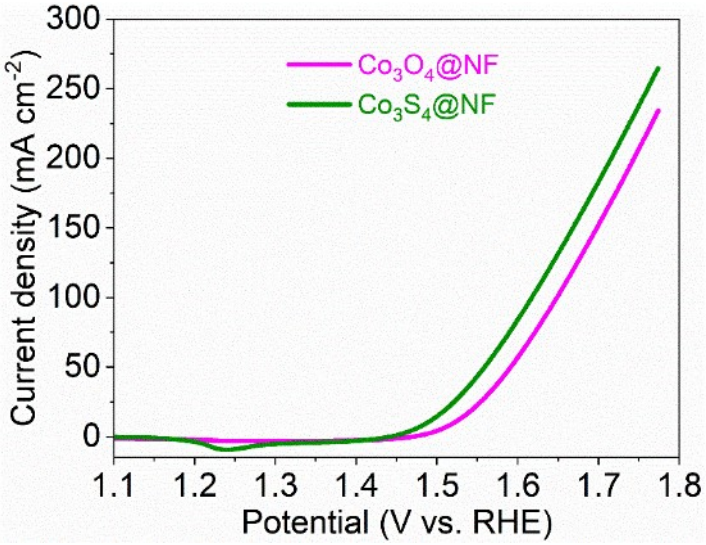

Fig. S10 LSV curves obtained by reverse scanning at a scan rate of 2 mV s^{-1}.

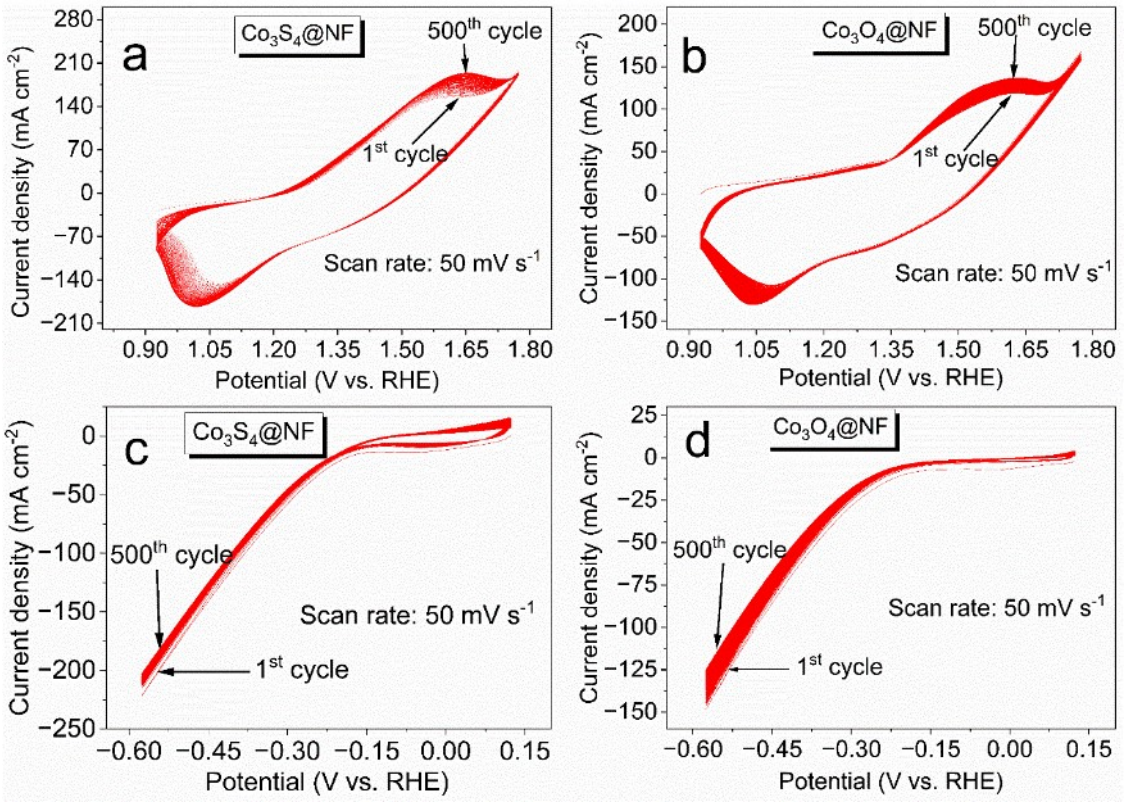

Fig. S11 Cyclic voltammograms of (a) Co_3S_4@NF in OER region, (b) Co_3O_4@NF in OER region, (c) Co_3S_4@NF in HER region, (d) Co_3O_4@NF in HER region for 500 cycles at a scan rate of 50 mV s^{-1}.

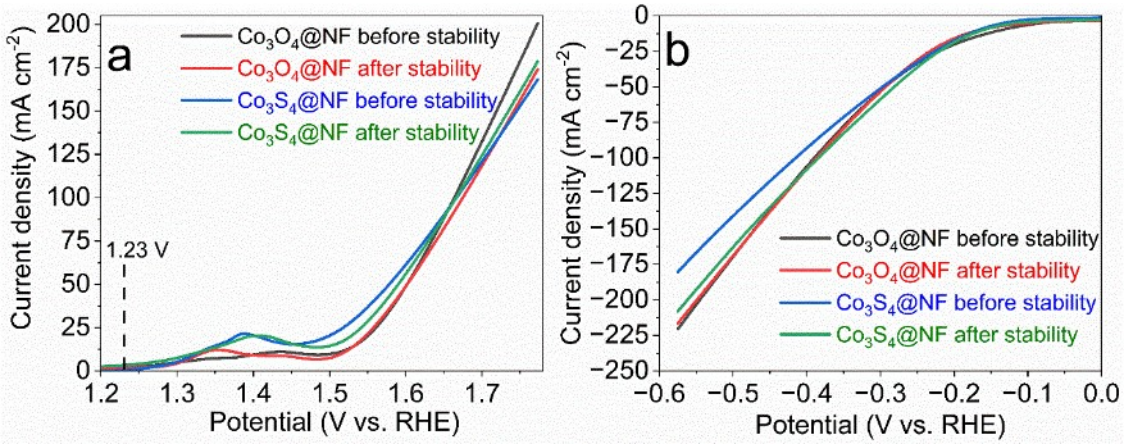

Fig. S12 LSV curves of Co_3O_4@NF and Co_3S_4@NF before and after stability for (a) OER, (b) HER at a scan rate of 2 mV s^{-1}.

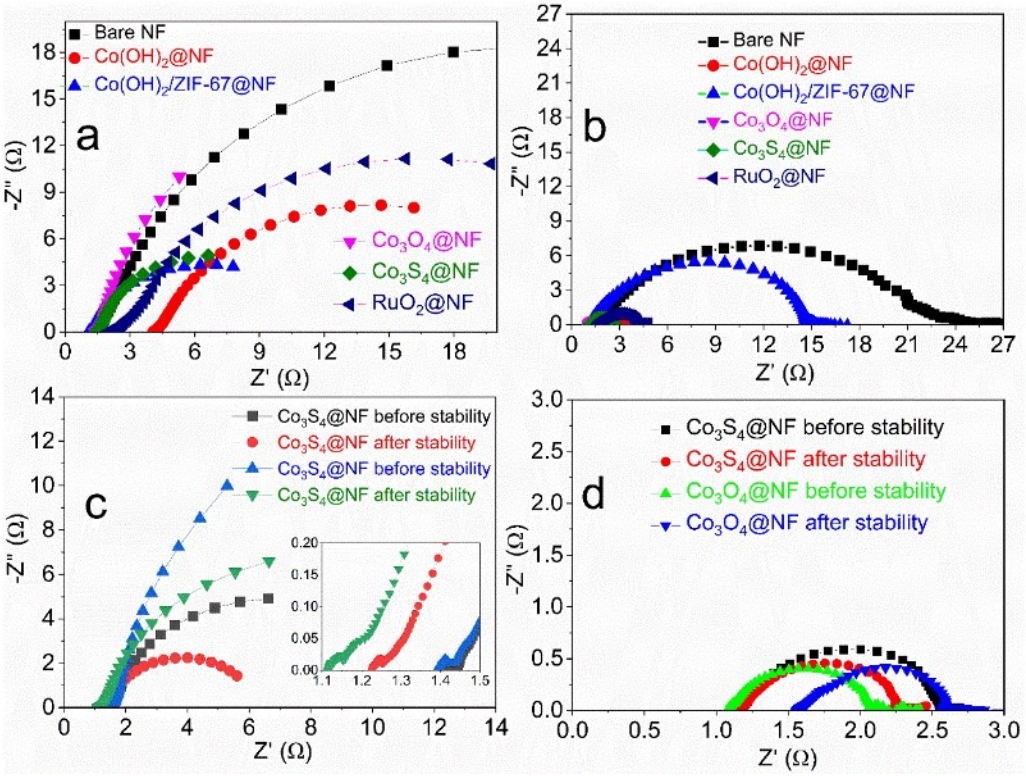

Fig. S13 Nyquist plots of synthesized materials (a) in OER region at 1.47 V (vs. RHE) before stability, (b) in HER region at -0.276 V (vs. RHE) before stability, (c) before and after stability in OER region at 1.47 V (vs. RHE), and (d) before and after stability in HER region at -0.276 V (vs. RHE).

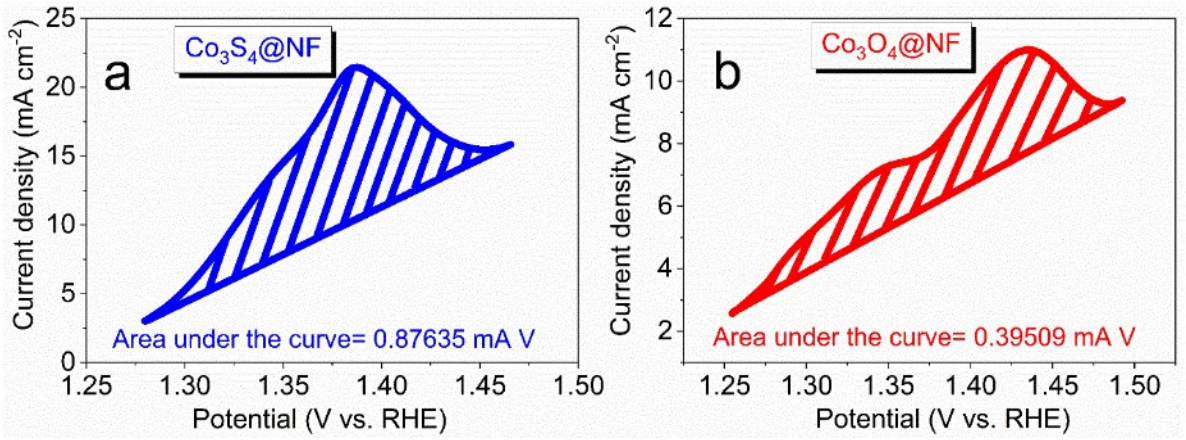

Fig. S14 Area under the oxidation peak of (a) Co_3O_4@NF, and (b) Co_3S_4@NF of the LSV curves at scan rate of 2 mV s^{-1}.

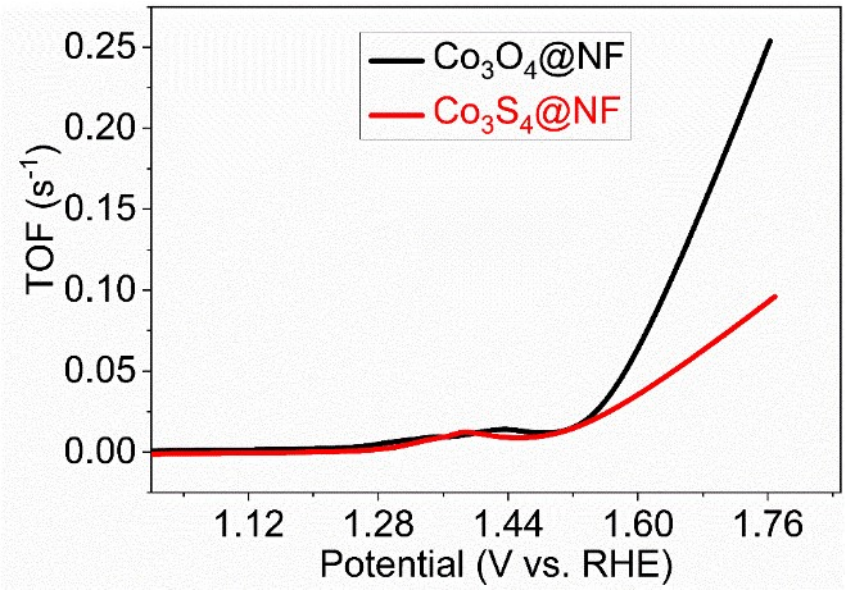

Fig. S15 The corresponding calculated TOF curves of the investigated catalysts.

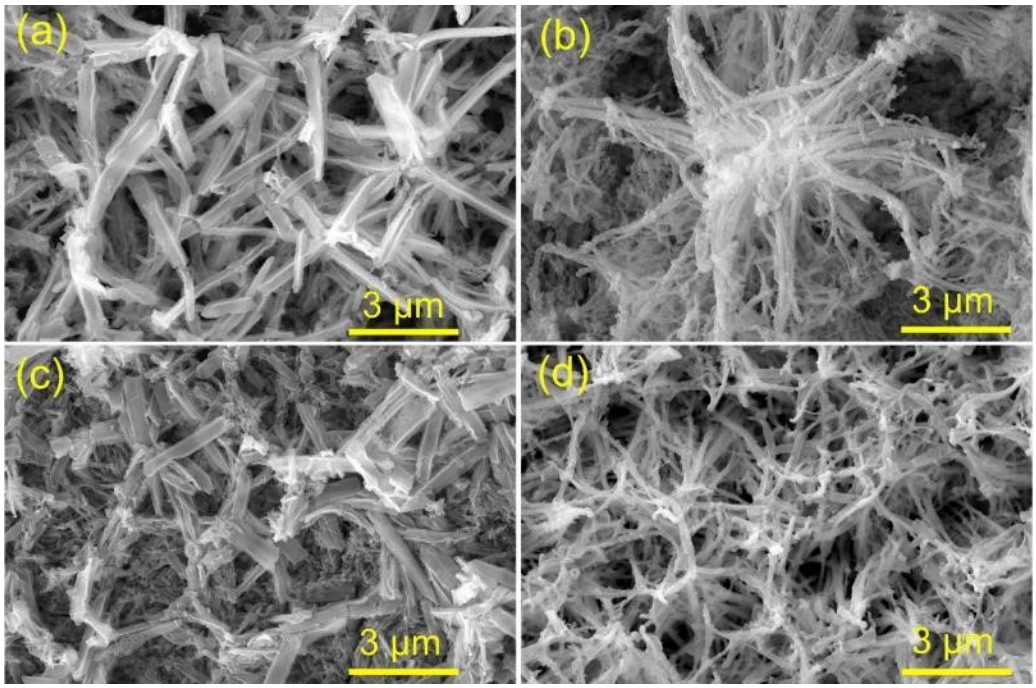

Fig. S16 The FE-SEM images of (a) Co_3O_4@NF after OER studies, (b) Co_3S_4@NF after OER studies, (c) Co_3O_4@NF after HER studies, and (d) Co_3S_4@NF after HER studies.

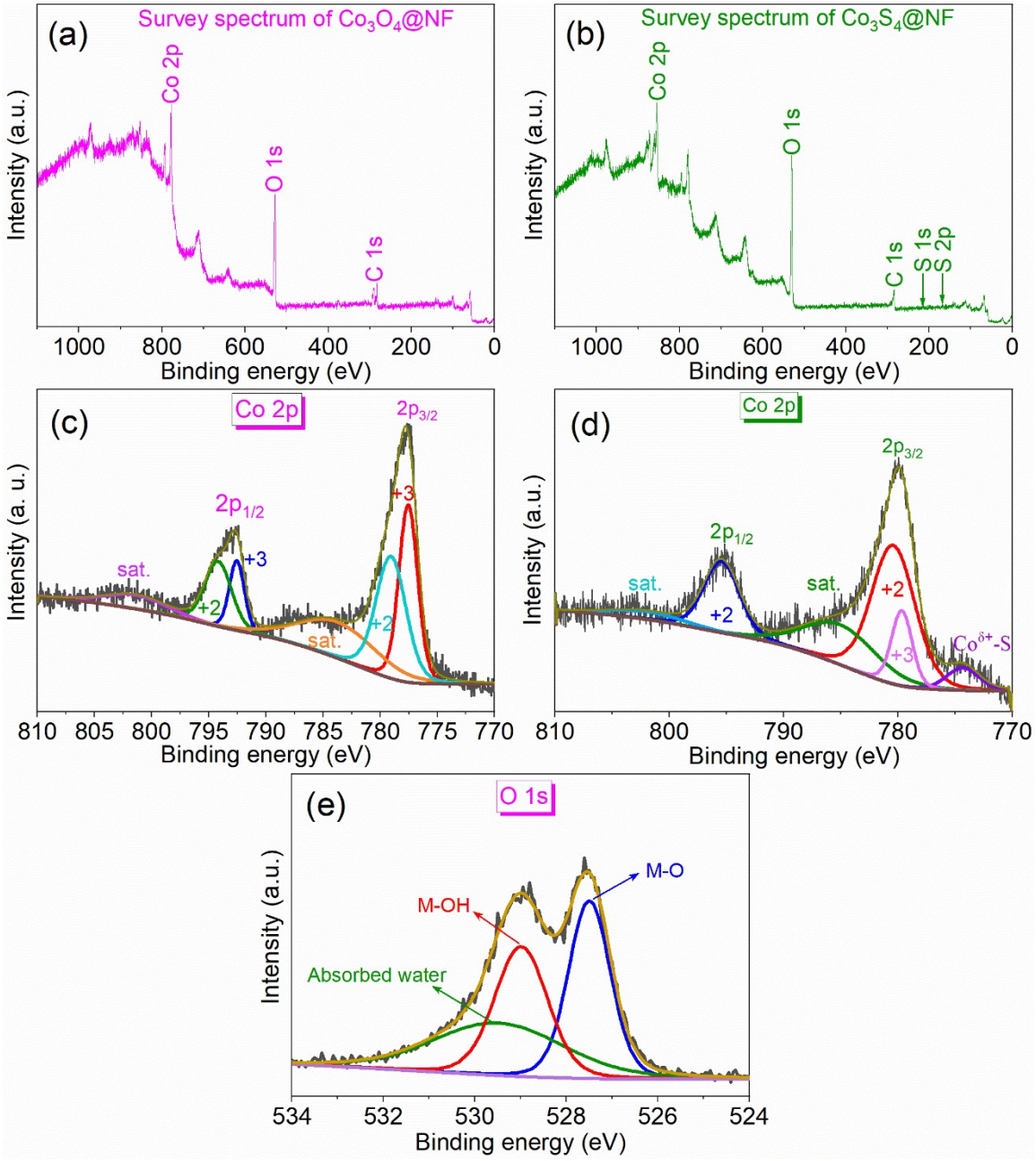

Fig. S17 XPS survey spectra after OER studies of (a) Co_3O_4@NF, (b) Co_3S_4@NF, and deconvoluted spectra for Co 2p of (c) Co_3O_4@NF, (d) Co_3S_4@NF, and (e) O 1s of Co_3O_4@NF.

Table S1. Tafel slope, overpotentials at current densities of 10 mA cm^{-2} and 20 mA cm^{-2} of the synthesized electrocatalysts for OER.

Electrocatalyst	Tafel slope ($mV\ dec^{-1}$)	η@10 mA cm^{-2} (mV)	η@20 mA cm^{-2} (mV)	Electrolyte
Bare NF	223	344	377	1 M KOH
$Co(OH)_2$@NF	215	293	334	1 M KOH
$Co(OH)_2$/ZIF-67@NF	173	265	304	1 M KOH
Co_3O_4@NF	132	270	318	1 M KOH
Co_3S_4@NF	189	-	260	1 M KOH
RuO_2@NF	182	317	359	1 M KOH

Calculation of exchange current density (j_0) from EIS:

For Co_3O_4@NF before stability for OER-

$$j_0 = (8.314\ J\ K^{-1}\ mol^{-1} \times 298\ K) \Big/ (4 \times 96485\ C\ mol^{-1} \times 1.452\ \Omega \times 1\ cm^2)$$

$$j_0 = 4.42\ mA\ cm^{-2}$$

For Co_3O_4@NF before stability for HER-

$$j_0 = (8.314\ J\ K^{-1}\ mol^{-1} \times 298\ K) \Big/ (2 \times 96485\ C\ mol^{-1} \times 1.452\ \Omega \times 1\ cm^2)$$

$$j_0 = 3.69\ mA\ cm^{-2}$$

Similarly, all j_0 values are calculated following above calculation process, and presented in the **Table S2**.

Table S2. Exchange current density (j_0) from EIS data.

Electrocatalyst	j_0 **for OER** **(mA cm^{-2})**	j_0 **for HER** **(mA cm^{-2})**
Co_3O_4@NF before stability	4.42	3.69
Co_3O_4@NF after stability	5.52	4.95
Co_3S_4@NF before stability	4.45	4.99
Co_3S_4@NF after stability	5.13	5.76
$Co(OH)_2$@NF	1.563	3.9
$Co(OH)_2$/ZIF-67@NF	5.825	0.878

Table S3. Nyquist plot data of synthesised materials in OER region at 1.47 V (vs. RHE) potential.

Electrocatalyst	R_s **(Ω)**	R_{ct} **(Ω)**	R_T **(Ω)**
Co_3O_4@NF before stability	1.390	0.062	1.452
Co_3O_4@NF after stability	1.115	0.047	1.162
Co_3S_4@NF before stability	1.414	0.028	1.442
Co_3S_4@NF after stability	1.225	0.027	1.252

$Co(OH)_2$@NF	4.0741	0.0319	4.106
$Co(OH)_2$/ZIF-67@NF	1.0859	0.0161	1.102

Table S4. Overpotential of synthesized materials before and after stability test for OER.

Electrocatalyst	**j (10 mA cm^{-2})**	**j (20 mA cm^{-2})**	**Ref.**
Co_3O_4@NF before stability	270	318	This work
Co_3O_4@NF after stability	280	315	This work
Co_3S_4@NF before stability	-	260	This work
Co_3S_4@NF after stability	253	292	This work

Table S5. Overpotential of synthesized materials before and after stability test for HER.

Electrocatalyst	**j (-10 mA cm^{-2})**	**j (-20 mA cm^{-2})**	**Ref.**
Co_3O_4@NF before stability	124	178	This work
Co_3O_4@NF after stability	154	195	This work
Co_3S_4@NF before stability	152	180	This work
Co_3S_4@NF after stability	149	181	This work

Table S6. Double layer capacitance (C_{dl}), electrochemically active surface area (ECSA) and roughness factor (RF) values of different synthesised electrocatalysts.

Electrocatalyst	Slope	C_{dl} (mF cm^{-2})	ECSA (cm^2)	RF
Bare NF	4.2	2.1	52.5	52.5
$Co(OH)_2$@NF	4.78	2.39	59.75	59.75
$Co(OH)_2$/ZIF-67@NF	3.38	1.69	42.25	42.25
Co_3O_4@NF	15.67	7.835	195.875	195.875
Co_3S_4@NF	28.39	14.195	354.875	354.875
RuO_2@NF	23.25	11.625	290.625	290.625

For the calculation of Turn Over Frequency (TOF):

Active site calculation is important to calculate TOF. Co^{3+} centres formed after oxidation of Co^{2+} are thought to be the potential active sites. The number of electrons involved in this Co^{2+}-Co^{3+} redox couple is only one. Hence, if we can calculate the charge (Q) involved in the transformation of Co^{2+} to Co^{3+}, we can calculate the total number of electrons involved in practical application of the electrocatalyst by dividing the total charge involved (Q) by the charge of one electron. Since, there is an involvement of only one electron, assuming all Co^{3+} centres to be active sites, we can assume the number of electrons involved to be equal to the total number of active sites in the electrocatalyst.

Calculation of active sites:

Area under the oxidation peak of LSV curve of the redox couple Co^{2+}-Co^{3+} of Co_3O_4@NF (**Fig. S14)** = 0.39509 mA V

Hence, $$Q = \frac{1}{v}\int_{E_1}^{E_2} i(E)\, dE \qquad (v = scan\ rate)$$

$$= {(0.39509\ mA\ V)}/{(0.002\ V\ s^{-1})} = 197.545\ mA\ s = 0.197545\ C$$

Number of electrons involved $$= {0.197545\ C}/{1.602 \times 10^{-19}\ C} = 1.233{\times}10^{18}$$

Hence, number of active sites in Co_3O_4@NF $= 1.233{\times}10^{18}$

Similarly, number of active sites in Co_3S_4@NF was calculated and found to be $= 2.735{\times}10^{18}$

The TOF was calculated from the integrated OER LSV curves at a scan rate of 2 mV s^{-1} using the equation (9) and shown in **Fig. S15**.

Tabel S7. Number of active sites and TOF of the electrocatalysts.

Electrocatalyst	**No. of active sites**	**Potential (V vs. RHE)**	**TOF (s^{-1})**
Co_3O_4@NF	$1.233{\times}10^{18}$	1.6	0.064
		1.76	0.25
Co_3S_4@NF	$2.735{\times}10^{18}$	1.6	0.035

	1.76	0.093

Table S8. Comparison of electrocatalytic OER performance of the Co_3O_4@NF and Co_3S_4@NF electrodes with recently reported non-precious transition metal based electrocatalysts.

Electrocatalyst	Electrolyte	j (mA cm^{-2})	η (mV)	Ref.
Co_3O_4@NF	1 M KOH	10 20	270 318	This work
Co_3S_4@NF	1 M KOH	20	260	This work
Co_3S_4@rGO	0.5 M H_2SO_4	10	350	S4
Co_3O_4@rGO	0.5 M H_2SO_4	10	380	S4
CoS_x/Ni_3S_2@NF	1 M KOH	20	280	S5
FeCoNiP@NC	1 M KOH	10	266	S6
Co-Fe oxyphosphide	1 M KOH	10	280	S7
Ni-Fe urchin-like catalyst	1 M KOH	10 20 100	292 318 374	S8
ZrNi-FeOOH	1 M KOH	10 100	231 250	S9
Fe-Ni_5P_4/NiFeOH-350	1 M KOH	10	221	S10
Ni-Ru@Fe/C@CNT	1 M KOH	10	246	S11
Fe-MOF/Au-8/FF	Alkaline	10	320	S12
Co@BNPCFs-800	1 M KOH	10	324	S13
Co/Mo_2C@C	1 M KOH	10	254	S14

CoMoNiPi	1 M KOH	10	272	S15
Co@CoMoOx-α-CrOOH	1 M KOH	10	278	S16
Co-NCNT@NHC	1 M KOH	20	300	S17
Co@NC nanocage/HCF_{200}	O_2 sat. 1 M KOH	10	396	S18
Ni-Fe-S	1 M KOH	10 50	375.3 450	S19

Table S9. Tafel slope, overpotentials at current densities of -10 mA cm^{-2} and -20 mA cm^{-2} of the synthesized electrocatalysts for HER.

Electrocatalyst	**Tafel slope ($mV\ dec^{-1}$)**	**η@-10 mA cm^{-2} (mV)**	**η@-20 mA cm^{-2} (mV)**	**Electrolyte**
Bare NF	200	253	298	1 M KOH
$Co(OH)_2$@NF	192	221	266	1 M KOH
$Co(OH)_2$/ZIF-67@NF	179	238	280	1 M KOH
Co_3O_4@NF	154	124	178	1 M KOH
Co_3S_4@NF	110	152	180	1 M KOH
Pt/C@NF	88	11	30	1 M KOH

Table S10. Nyquist plot data of synthesised materials in HER region at -0.3 V (vs. RHE) potential.

Electrocatalyst	R_s **(Ω)**	R_{ct} **(Ω)**	$\mathbf{R_T}$ **(Ω)**

Co_3O_4@NF before stability	1.16	2.32	3.48
Co_3O_4@NF after stability	1.56	1.03	2.59
Co_3S_4@NF before stability	1.16	1.41	2.57
Co_3S_4@NF after stability	1.16	1.11	2.27
$Co(OH)_2$@NF	1.402	1.89	3.292
$Co(OH)_2$/ZIF-67@NF	1.129	13.989	14.619

Table S11. Comparison of electrocatalytic HER performance of the Co_3O_4@NF and Co_3S_4@NF electrodes with recently reported non-precious transition metal based electrocatalysts.

Electrocatalyst	**Electrolyte**	**-j (mA cm^{-2})**	**η (mV)**	**Ref.**
Co_3O_4@NF	1 M KOH	10 20	124 178	This work
Co_3S_4@NF	1 M KOH	10 20	152 180	This work
Co_3S_4@rGO	0.5 M H_2SO_4	10	151	S4
Co_3O_4@rGO	0.5 M H_2SO_4	10	234	S4
CoS_x/Ni_3S_2@NF	1 M KOH	10	204	S5
FeCoNiP@NC	1 M KOH 0.5 M H_2SO_4	10 10	187 93	S6
Co-Fe oxyphosphide	1 M KOH	10	180	S7
Ni-Fe urchin-like catalyst	1 M KOH	10	124	S8

		20 100	157 243	
ZrNi-FeOOH	1 M KOH	10 100	150 273	S9
Fe-Ni_5P_4/NiFeOH-350	1 M KOH	10	197	S10
Fe-MOF/Au-8/FF	Alkaline	10	130	S12
Co@BNPCFs-800	1 M KOH	10	151.3	S13
Co-NCNT@NHC	1 M KOH	10	180	S17
Co@NC nanocage/HCF_{200}	N_2 sat. 1 M KOH	10	261.4	S18
$ZnCo_2S_4/CoZn_{13}$	Alkaline	10	160	S20
NiFeCo-LDH/CF	1 M KOH	10	151	S21
$Zn_{1-x}Fe_x$-LDH/Ni-foam	1 M KOH	10	221	S22

Table S12. Comparison of cell potential needed for overall water splitting with recently reported electrode materials.

Electrode material (Cathode)	**Electrode material (Anode)**	**j (mA cm^{-2})**	**Cell potential (V)**	**Electrolyte**	**Ref.**
MoS_2/NiFe-LDH	MoS_2/NiFe-LDH	10	1.61	1 M KOH	S1
Co(OH)F@CoFe-LDH	Co(OH)F@CoFe-LDH	10	1.58	1 M KOH	S2
NiFeOP	NiFeOP	10	1.57	1 M KOH	S3
Co_3S_4@rGO	Co_3S_4@rGO	10	1.82	0.5 M H_2SO_4	S4

CoS_x/Ni_3S_2@NF	CoS_x/Ni_3S_2@NF	10 50	1.572 1.863	1 M KOH	S5
FeCoNiP@NC	FeCoNiP@NC	10	1.73	1 M KOH	S6
$Zn_{1-x}Fe_x$-oxyselenide/Ni-foam	$Zn_{1-x}Fe_x$-oxyselenide/Ni-foam	10	1.62	1 M KOH	S22
Co_3O_4@NF	Co_3S_4@NF	10 20 50	1.63 1.72 1.83	1 M KOH	This work
Co_3O_4@NF	Co_3O_4@NF	10 20 50	1.61 1.76 1.88	1 M KOH	This work
Co_3S_4@NF	Co_3S_4@NF	10 20 50	1.63 1.80 1.96	1 M KOH	This work

References

S1 X.-P. Li, L.-R. Zheng, S.-J. Liu, T. Ouyang, S. Ye, and Z.-Q. Liu, *Chin. Chem. Lett.*, 2022, **33**, 4761-4765.

S2 M. Qin, Y. Wang, H. Zhang, M. Humayun, X. Xu, Y. Fu, M. K. Kadirov and C. Wang, *CrystEngComm*, 2022, **24**, 6018–6030.

S3 Y. Xie, B. Zhao, K. Tang, W. Qin, C. Tan, J. Yao, Y. Li, L. Jiang, X. Wang, and G. Zou, *Chem. Eng. J.*, 2021, **409**, 128156–128156.

S4 R. S. Kumar, S. C. Karthikeyan, S. Ramakrishnan, S. Vijayapradeep, A. R. Kim, J.-S. Kim and D. J. Yoo, *Chem. Eng. J.* **2023**, *451*, 138471.

S5 S. Shit, S. Chhetri, W. Jang, N. C. Murmu, H. Koo, P. Samanta, and T. Kuila, *ACS Appl. Mater. Interfaces*, 2018, **10**, 27712–27722.

S6 J. Sun, S. Li, Q. Zhang, and J. Guan, *Sustain. Energy Fuels*, 2020, **4**, 4531–4537.

S7 P. Zhang, X. Lu, J. Nai, S.-Q. Zang, and W. David, *Adv. Sci.*, 2019, **6**, 1900576–1900576.

S8 E. Hatami, A. Toghraei and G. B. Darband, *Int. J. Hydrog. Energy*, 2021, **46**, 9394–9405.

S9 Y. Yan, J. Liu, S. Feng, S. Ding, L. Qiao, X. Zheng, and W. Cai, *J. Mater. Chem. A*, 2021, **9**, 26777–26787.

S10 C.-F. Li, J.-W. Zhao, L.-J. Xie, J.-Q. Wu and G.-R. Li, *Appl. Catal.*, 2021, **291**, 119987.

S11 T. Gao, X. Li, X. Chen, C. Zhou, Q. Yue, H. Yuan, and D. Xiao, *Chem. Eng. J.*, 2021, **424**, 130416–130416.

S12 Y. Xu, M. Xie, L. Xianfa, F. Shao, S. Li, S. Li, Y. Xu, J. Chen, F.-G. Zeng and Y. *J.* Jiao, *Interface Sci.*, 2022, **626**, 426–434.

S13 F. Guo, Z. Liu, J. Xiao, X. Zeng, C. Zhang, Y. Lin, P. Dong, T. Liu, Y. Zhang and M. Li, *Chem. Eng. J.*, 2022, **446**, 137111.

S14 S. Yuan, M. Xia, Z. Liu, K. Wang, L. Xiang, G. Huang, J.-Y. Zhang, and N. Li, *Chem. Eng. J.*, 2022, **430**, 132697–132697.

S15 R. Ramaraj, and K. Kim, *ACS Appl. Mater. Interfaces*, 2023, **15**, 16571–16583.

S16 S. F. Lim, C.-L. Chiang, C.-K. Peng, W. Wu, Y.-C. Lin, Y.-R. Lin, C.-L. Chen and Y.-G. Lin, *Chem. Eng. J.*, 2022, **452**, 139715–139715.

S17 Y. Zhuang, H. Cheng, C. Meng, B. Chen and H. Zhou, *J. Colloid Interface Sci.*, 2023, **643**, 162–173.

S18 R. Zhu, X. Yu, W. Li, M. Li, X. Bo, and G. Gan, *J. Alloys Compd.*, 2023, **947**, 169488.

S19 W. Xu, S. Zhao, J.-P. Zhang, X. Yang, Y.-X. Tang, Y.-W. Han, and Y. Shen, *Int. J. Hydrog. Energy*, 2023, **48**, 18315-18325.

S20 D. Zhao, M. Dai, H. Liu, Z. Duan, X. Tan, and X. Wu, *J. Energy Chem.*, 2022, **69**, 292–300.

S21 R. Hu, H. Jiang, J. Xian, S. Mi, L. Wei, G. Fang, J. Guo, S. Xu, Z. Liu, H. Jin, H. Yu, and J. Wan, *Nanomaterials*, 2022,**12**, 2416–2416.

S22 G. Rajeshkhanna, S. Kandula, K. R. Shrestha, N. H. Kim and J. H. Lee, *Small*, 2018, **14**, 1803638.